JOURNAL OF APPLIED PHYSICS VOLUME 86, NUMBER 7 1 OCTOBER 1999

Accurate determination of pulsed current waveform in plasma immersion ion implantation processes

Xiubo Tian, Baoyin Tang, and Paul K. Chu[a)]
Department of Physics and Materials Science, City University of Hong Kong, 83 Tat Chee Avenue, Kowloon, Hong Kong

(Received 20 October 1998; accepted for publication 24 June 1999)

This article reports on the measurement of the ion current in plasma immersion ion implantation. Our simulation results indicate that the total current peaks at the end of rise time of the applied voltage. However, our experimental data acquired using a Rogowski coil and digital oscillator show the highest current at the beginning of the voltage pulse. The discrepancy can be explained by a displacement current attributable to the changing voltage, sheath capacitance, circuit loading effects, as well as secondary electron emission. © *1999 American Institute of Physics.*
[S0021-8979(99)02919-9]

I. INTRODUCTION

Plasma immersion ion implantation (PIII) is a promising alternative to conventional beam-line ion implantation for the surface modification of materials and industrial components. PIII eliminates the need of beam rastering because the entire target is immersed in a plasma.[1–3] Therefore, PIII offers unique advantages when treating non-planar surfaces or samples of an irregular shape. Improvements in surface hardness, wear, and corrosion resistance after PIII treatment are well documented in the literature.[4–6]

During the PIII process, the implantation voltage and current waveforms must be monitored closely to ensure proper instrument operation. In addition, information such as the implantation dose, sheath condition, target temperature, and secondary electron emission coefficient can be deduced from the waveforms.[7] Hence, accurate current waveform measurement is crucial to the success of PIII. The total current waveform is composed of both the ion current as well as the secondary electron current. The latter component is quite large, especially at higher ion impact energies. In this article, we present our experimental results and compare them to the theoretical waveforms generated by our model. The discrepancy can be explained by a displacement current arising from the pulse modulator. We will also present a correction method to more accurately determine the current waveform.

II. THEORETICAL SIMULATION

In PIII, a negative voltage pulse is applied to the target. On the time scale of the inverse electron plasma frequency, electrons adjacent to the implanted surface are repelled leaving behind a uniform density ion matrix sheath. Subsequently, on the time scale of the inverse ion plasma frequency, ions within the sheath are accelerated towards the target. This, in turn, drives the edge of the plasma sheath further away implanting more ions. On a longer time scale, the system evolves towards a steady-state Child–Langmuir law sheath.[8,9]

[a)]Electronic mail: paul.chu@cityu.edu.hk

To simulate the sheath dynamics several assumptions are made including the implantation current, secondary electron current, and sheath expansion. In a typical PIII process, ions within the sheath are accelerated to thousands of eV resulting in a transient time on the order of nanoseconds. Thus, the sheath transient time is instantaneous when compared to the voltage pulse typically in the range of microseconds. Under low pressure conditions (sub-mTorr regime), collisionless conditions are valid and all ions within the sheath do not undergo collision or charge transfer and are implanted at the applied voltage. Since the sheath voltage is always greater than the electron temperature, we can assume that a quasi-static Child–Langmuir law sheath exists at all times and the ion current is spatially constant within the sheath. As a result, when a negative voltage is applied to the target, a dynamic process will commence. The primary electrons are pushed away, an ion sheath forms, ions are implanted into the target at an applied voltage that varies in the beginning depending on the slew rate of the power modulator, and secondary electrons are induced. Meanwhile the electrons in the plasma continue to be repelled to the anode as the sheath evolves. The total current thus has several components:[10–13]

A. Implantation current (J_i)

J_i can be described using the Child–Langmuir law. For a voltage V_a across a collisionless sheath of thickness S, the current is

$$J_i=\frac{4}{9}\varepsilon_0 A\left(\frac{2q}{M}\right)^{1/2}\frac{V_a^{3/2}}{S^2}, \tag{1}$$

where ε_0 is the free-space permittivity, q is the ion charge, A is the exposed surface area, and M is the ion mass.

B. Secondary electron current (J_s)

For a substance with a high secondary electron yield such as Al_2O_3, the secondary electron can dominate the total current at high voltage. The secondary electron yield as a function of the ion energy has been measured in a glow

 © 1999 American Institute of Physics

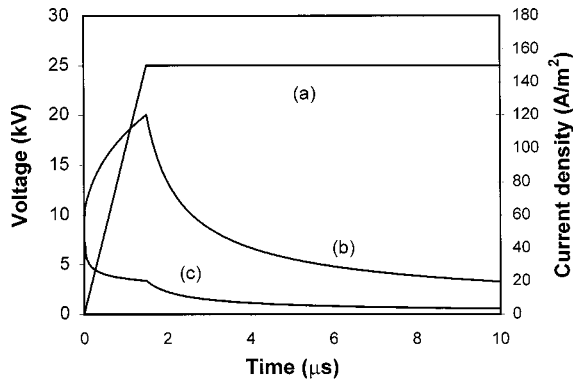

FIG. 1. Simulated time-dependent voltage and current waveforms: (a) voltage, (b) total current, (c) ion current.

discharge[14] and under PIII conditions.[7] The secondary electron emission coefficient is generally proportional to the square root of the applied voltage V_a:

$$\gamma = k(V_a)^{1/2}, \tag{2}$$

where k is measured experimentally. The secondary electron current is

$$J_s = \gamma J_i = f(V_a). \tag{3}$$

C. Plasma electron current (J_e)

In the plasma, it is assumed that the electrons have a single Maxwellian distribution with temperature T_e. Hence, the electron current, J_e, is

$$J_e = \tfrac{1}{4} e n_0 A u_e e^{-V_a/T_e}, \tag{4}$$

where n_0 is the plasma density and u_e is the average electron velocity equal to

$$u_e = (8eT_e/\pi m_e)^{1/2}. \tag{5}$$

In our sheath dynamics simulation, it is assumed that the ion current, J_i, arises from both the uncovering of ions due to the movement of the sheath edge and the flow of ions toward the target. Therefore,

$$J_i = q n_0 A\left(\frac{ds}{dt} + \nu_d\right), \tag{6}$$

where ν_d is the ion acoustic speed.

The ion sheath characteristics including the ion current and total current can be derived by numerically solving the Child–Langmuir equation. To simulate a real situation, we use typical values determined experimentally, e.g., ion density $n_0 = 5\times10^9$ ions/cm^3, voltage $V_a = -25$ kV, and a linear rise time $t_s = 1.5$ μs. For simplicity, the latter part of the voltage waveform is ignored in our simulation and some of the experiments. As shown in Fig. 1 (curve c), the simulated ion current is highest in the beginning of the voltage pulse and then decreases quite rapidly. In contrast, the maximum total current or effective current, I_{eff}, appears at the end of the rise time (curve b). The simulation results indicate that the total current can be divided into three time domains. In region 1 that represents the beginning of the voltage pulse, the current is composed of mostly ion current because the secondary electron current is very small owing to the low ion energy. In region 2, the total current gradually increases in spite of the rapidly diminishing ion current. The contribution from secondary electrons becomes progressively larger. In region 3, the applied voltage becomes constant and the effective current begins to decrease with time as ions are depleted from the sheath. The total current will finally attain a stable value corresponding to a steady Child–Langmuir law sheath. A closer look at the ion current and total current waveforms reveals an inflection point that is brought about by the assumed trapezoidal voltage waveform. Experimentally, curve b is most important because it represents the total current and is the measured parameter in a PIII process.

III. EXPERIMENT

In general, PIII experiments are conducted between 10 and 80 kV and the current can be quite large. For our work, in order to conduct high voltage, high current measurements, a capacitance divider (Pearson model 305A) and Rogowski coil (Pearson model 110) were employed. A digital oscillator (Tektronix TDS360) was also used to save and restore voltage and current data via our distributive controller reported earlier.[15] A hard tube (TM702) was used in the modulator as a switch to directly provide the target a negative high voltage, and a description of the apparatus can be found elsewhere.[2] The voltage was adjusted by the screen and control grids. The bias voltage of the screen grid was fixed at 2 kV. The voltage on the control grid determined the dynamic behavior of the output voltage. For example, a higher voltage could lead to a shorter rise time but bigger ringing of the output voltage. The voltage and current were measured near the anode of the hard tube, from which a 2.5 m long high voltage cable was connected to the target. The connecting cable was fed through a high voltage feedthrough filled with oil for cooling. In our experiments, the nitrogen plasma was generated by hot filament glow discharge. The density was typically about 5×10^9/cm^3 unless specified otherwise. The sample chuck consisted of a 100-mm-diam, 5-mm-thick round platen supported by an 8-mm-diam rod. The applied voltage was varied from 10 to 30 kV and the rise time was in the range of 0.5–3.0 μs. The pulse duration was 10–30 μs and the implantation frequency was 300 Hz. To observe the plasma sheath response to the applied voltage and pulse duration, we also conducted experiments using a longer pulse duration: sample biasing voltage $= -10$ kV, pulse width $=200$ μs, and pulsing frequency $=100$ Hz.

IV. RESULTS AND DISCUSSION

Figure 2 displays the voltage and current waveforms acquired from the long pulse duration experiment. The low implantation voltage and long pulse duration were chosen to reflect the real dynamic process including the formation of the steady Child–Langmuir sheath. As shown, the current waveform clearly indicates the ion sheath dynamic process described by the Child–Langmuir law. Initially, a high current appears owing to a small sheath. As the sheath expands, the current diminishes. Eventually, the sheath achieves an

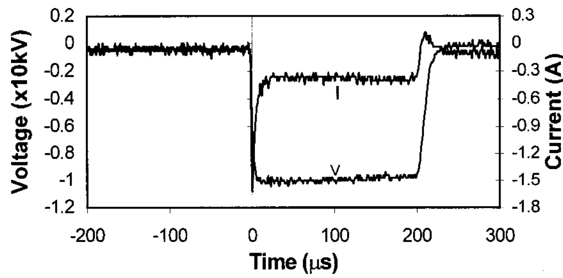

FIG. 2. Experimental time-dependent voltage and current waveform.

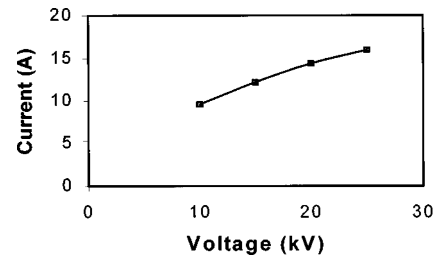

FIG. 4. Measured displacement current vs applied voltage.

equilibrium value leading to a constant current that depends on the ion acoustic velocity v_d. For an infinite plane, this is described by the following equation:[8,13]

$$I=(1+\gamma)en_0v_dA. \tag{7}$$

The sheath rests at S_c and can be calculated by

$$S_c=S_0\left[\frac{2}{9}\left(\frac{u_0}{V_d}\right)\right]^{1/2}, \tag{8}$$

where $S_0=(2\varepsilon_0V_a/en_0)^{1/2}$ is the matrix sheath thickness and $u_0=(2eV_a/M)^{1/2}$ is the characteristic ion velocity.

In our current analysis shown in Fig. 3, we focus on the initial part of the current waveform. The measured total current peaks at the beginning of the voltage pulse, and then decreases precipitously finally achieving dynamic equilibrium. Our data also indicate that the electrical load on the power modulator is indeed capacitive.

The measured current waveform exhibited in Fig. 2 or Fig. 3(a) is quite different from the theoretical current waveform shown as curve b in Fig. 1, in spite of the different voltages. Conventional wisdom is that only when a high voltage is applied to the plasma will there be ion current and secondary electron current. However, the measured current waveform does not support the logic. To explain the discrepancy, we will use the concept of a displacement current. The current measured by the Rogowski coil is the total current flowing between the cathode (target) and anode (earth). When a negative high voltage is imposed, the vacuum chamber, sheath, and electrical circuit inherently induce an equivalent capacitive load for the modulator inevitably giving rise to a displacement current. That is, a displacement current results due to the changing voltage, sheath capacitance, and circuit loads. To obtain this displacement current data, we can use the method suggested by Shamim *et al.*[16] and Chen *et al.*[17] The displacement current, I_d, can be measured by applying pulses of high negative voltage to the target without a plasma (sheath capacitance is assumed to be negligible). We can then obtain the effective current component, I_{eff}, by subtracting Fig. 3(b) (current without plasma) from Fig. 3(a) (current with plasma). As shown in Fig. 3(c), the resulting current waveform agrees well with the simulated waveform. The maximum current peaks at about 1.5 μs and the three regions described previously are quite apparent in the processed waveform. It shows that the ion current as well as secondary electron current form after a negative voltage is applied. The proposed correction method thus enables a more accurate measurement of the effective current

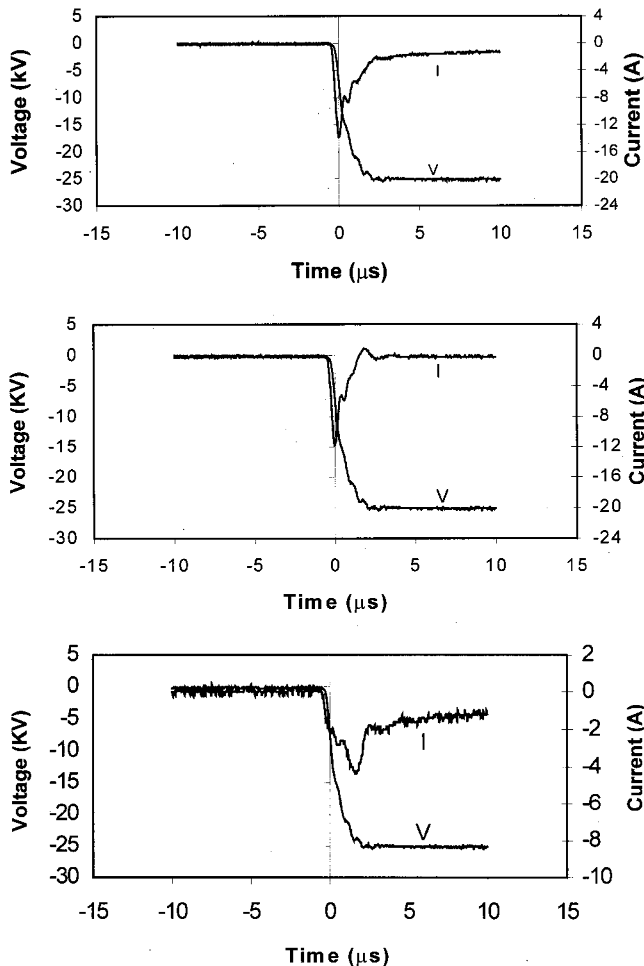

FIG. 3. Experimental time-dependent current waveform: (a) with plasma, (b) without plasma, (c) processed (subtracted) current. Only the first 10 μs of the pulse is shown.

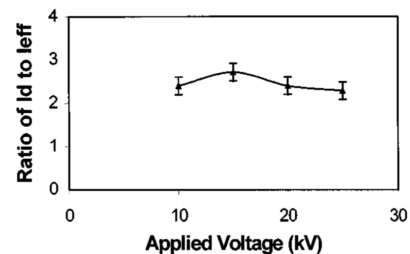

FIG. 5. Ratio of displacement current peak to effective current peak as a function of the applied voltage.

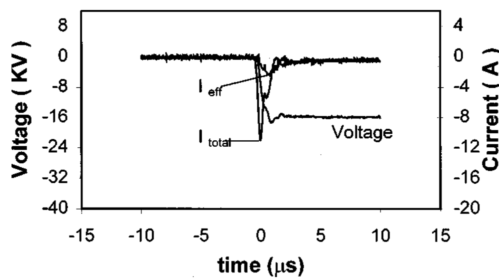

FIG. 6. Voltage and current waveforms at 15 kV biasing voltage and $2\times10^9/\mathrm{cm}^3$ plasma density.

which can subsequently be used to estimate the implant dose, sheath condition, and to predict the target temperature and so on.

By comparing the measured and processed current waveforms [Figs. 3(b) and 3(c)], we can conclude that the displacement current is very high. The current measured experimentally is thus dominated by the displacement current, especially at the initial stage of the applied voltage pulse, thus signifying the importance of this correction method. To study the characteristics of the displacement current, Fig. 4 shows that the measured displacement current increases almost linearly with the implantation voltage. However, as shown in Fig. 5, the displacement current to effective current ratio (I_d/I_{eff}) is over two and does not vary significantly with the applied voltage throughout this range. As the magnitude of this displacement current can be quite large, it must be taken into account when trying to calculate the real current from the experimental current waveform.

We have also investigated the case at a lower plasma density of about $2\times10^9/\mathrm{cm}^3$ and voltage of 15 kV. The total and effective current waveforms are illustrated in Fig. 6. The data are very similar to those obtained from the other experiments. Hence, the phenomenon that the current peaks near the end of the rise time is independent of the parameters in our experimental conditions (at least those used in this work). Our experimental results, particularly that concerning the effective current waveform, agree with our simulation results. It should be noted that the simulation is conducted using a one-dimensional model, that is, one describing an infinite planar target. We have only demonstrated the phenomenon and concept while we have not calculated exactly the spatial and time variations in case of a real sample with a finite size and irregular shape. However, our results show that secondary electrons alter the effective current waveform.

V. CONCLUSION

Accurate measurement of the effective current is very important in PIII processes. The presence of a displacement current makes it difficult to accurately derive the effective current from the total current waveform. We have experimentally determined the magnitude of this component in our equipment as well as its relationship with implantation voltage using a Rogowski coil and digital oscillator. To obtain a more accurate effective current waveform, the waveform without a plasma load must be subtracted. The resulting waveform is in good agreement with the theoretical simulation results showing the maximum net effective current at about the end of the pulse rise time. The simulation and experimental results demonstrate that while secondary electrons exert a minimal influence on the sheath expansion because they possess high velocities and can hardly react with the particles (ions, neutrals, etc.) in the sheath, they alter the effective current waveform. The ratio of the displacement current to the ion current is over 2 under our experimental conditions. Since the displacement current is larger than the effective current, accurate ion current determination will not be possible without correction. Reduction of the absolute displacement current requires careful design of the power modulator supply and understanding of its interaction with the various components in the system.

ACKNOWLEDGMENTS

The work was supported by Hong Kong RGC Earmarked Grant Nos. 9040332 and 9040344 as well as City University of Hong Kong Strategic Research Grant No. 7000964.

[1] J. R. Conrad, J. I. Radtke, R. A. Dodd, F. J. Worzala, and N. C. Tran, J. Appl. Phys. **62**, 4591 (1987).
[2] P. K. Chu, B. Y. Tang, Y. C. Cheng, and P. K. Ko, Rev. Sci. Instrum. **68**, 1886 (1997).
[3] P. K. Chu, S. Qin, C. Chan, N. W. Cheung, and L. A. Larson, Mater. Sci. Eng. **R17**, 207 (1996).
[4] B. Y. Tang, P. K. Chu, S. Y. Wang, K. W. Chow, and X. F. Wang, Surf. Coat. Technol. **103–104**, 248 (1998).
[5] S. Y. Wang, P. K. Chu, B. Y. Tang, X. B. Tian, X. F. Wang, and Q. Z. Lin, Thin Solid Films **311**, 190 (1997).
[6] S. Y. Wang, P. K. Chu, B. Y. Tang, J. C. Yan, and X. C. Zeng, Surf. Coat. Technol. **98**, 897 (1998).
[7] W. En and N. W. Cheung, IEEE Trans. Plasma Sci. **24**, 1184 (1996).
[8] M. A. Lieberman, J. Appl. Phys. **66**, 2926 (1989).
[9] R. A. Steward and M. A. Lieberman, J. Appl. Phys. **70**, 3481 (1991).
[10] W. En and N. W. Cheung, IEEE Trans. Plasma Sci. **44**, 379 (1997).
[11] B. P. Linder and N. W. Cheung, IEEE Trans. Plasma Sci. **24**, 1383 (1996).
[12] W. En, M. A. Lieberman, and N. W. Cheung, IEEE Trans. Plasma Sci. **23**, 415 (1995).
[13] J. T. Scheuer, M. Shamim, and J. R. Conrad, J. Appl. Phys. **67**, 1241 (1990).
[14] B. Szapirio and J. J. Rocca, J. Appl. Phys. **65**, 3713 (1989).
[15] A. G. Liu, X. F. Wang, B. Y. Tang, and P. K. Chu, Rev. Sci. Instrum. **69**, 1495 (1998).
[16] M. M. Shamim, J. T. Scheuer, R. P. Fetherston, and J. R. Conrad, J. Appl. Phys. **70**, 4756 (1991).
[17] A. Chen, J. Firmiss, and J. R. Conrad, J. Vac. Sci. Technol. B **12**, 918 (1994).